Calculation of Three - Phase Flow Behavior and its Influence on Reservoir Performance

Guzman R. E., Fayers F. J.

Stanford University, U. S. A.

Abstract

In this paper we study the effects of variations in relative permeabilities for three-phase flow on predicted oil and gas production behavior when immiscible gas displacement is used to enhance oil recovery from waterflooding. A 3-D model for a repeated 5-spot pattern provides a basis to analyze oil and gas-phase saturation distributions, and to estimate the volumetric extent of the reservoir experiencing three-phase flow conditions. Four variants of the Stone's I and II oil relative permeability models are used and shown to give significant differences in oil and gas production histories. The influences of including water/oil and gas/oil capillary pressures are examined. New definitions are given for capillary and gravity numbers for three-phase flows, and an approach suggested for calculating vertical equilibrium pseudos when gravity and capillary numbers are large. However, for the tested 5-spot examples, neither segregated flow nor capillary/gravity equilibrium conditions were found to occur and comparatively successful results were obtained from a relatively coarse vertical grid without adjusting the original rock relative permeability curves.

1. Introduction

Assumptions are made about three-phase flow in nearly all forms of simulators, including black oil, compositional/miscible gas, surfactant, and thermal models. In spite of this universal application, we have remarkably little knowledge about the mathematical, physical, or practical significance of selecting three-phase relative permeabilities. For example, we know that the occurrence of elliptic regions in the characteristics of the flow equations can be influenced by the choice of relative permeability models[1,2]. In gas displacement studies, the argument is sometimes made that the extent of the reservoir region experiencing three-phase flow conditions is quite small, so that the properties of these relative permeabilities would not have much practical significance. An elegant theory for semi-analytical solutions of three-phase flow behavior has recently been given by Virnovsky *et al.*[3], which relies on the assumption that all three phases have vertical distributions with essentially complete segregation. New solutions for three-phase Buckley-Leverett problems with gravity have recently been developed by Guzman[2]

Part of the purpose of this paper is to investigate in a 3-D repeated 5-spot example the extent of the three-phase flow regions, and how these depend on the choice of various Stone's models for the middle-phase oil relative permeability. The consequent variations in oil and gas production behaviors are compared, where the gas-phase production is found to be unexpectedly sensitive. The effects of including

capillary pressures are examined. New scaling criteria are introduced for three-phase flow, to estimate displacement rates at which the gravity and capillary forces should become significant. Although capillary pressures increase the size of the three-phase flow region, the production behaviors were not strongly influenced.

One further difficulty in modeling three-phase flow in large reservoir applications is associated with the choice of method for evaluating pseudo-relative permeabilities. Conceptually, the standard Kyte and Berry method[4] can be easily extended, but this does not readily provide relative permeabilities for water and gas which are monotonic functions of a single saturation for each of these two phases. Most reservoir simulators demand this characteristic in their numerical methods for three-phase flow. An apparently attractive alternative for calculating pseudos, which does satisfy the single saturation monotonic restrictions, can be obtained from assuming vertical equilibrium[5,6] saturation distributions independently for each coarse grid cell. We give an outline of this theory and analyze its potential for this kind of reservoir problem.

2. Model Description

The 3D homogeneous reservoir model selected for simulation with the ECLIPSE[7] code was one eighth of a repeated 5-spot pattern. The well spacing is 304.8 m (1000 ft) and the reservoir thickness 30.48 m (100 ft), with k_h = 100 mD and $k_v / k_h = 0.2$. Numerical experiments were performed on gridding details, and it was found that a diagonal grid of 25 x 13 x 25 (see Figure 4) gave a reasonable compromise on accuracy and execution time for the range of cases to be analyzed. 25 intervals in Δz were used to give adequate accuracy on gravity segregation tendencies between the three phases. The oil phase properties for the base case were $\mu_o = 2.0cP$, $\rho_o = 0.7$ gm/cm^2, and the gas phase, $\mu_g = 0.02cP$, $\rho_g = 0.001$ gm/cm^3. The gas/oil viscosity ratio is very adverse, as might apply to a dry gas injection process. Solution gas effects are ignored in this study. Further details on the fluid properties are given in Ref. 8. Some 50% of the calculations performed refer to displacement with water injection up to breakthrough, followed by gas injection. In the other half of the cases, the subsequent gas injection is applied in a WAG mode, with water and gas injected simultaneously with a WAG ratio of 1:1.

It was felt desirable to choose input two-phase relative permeabilities on a consistent basis which would be appropriate for imbibition of water (water-wet rock) and drainage displacement by gas. Thus the Standing expressions were adopted (see Appendix B of Ref. 8) with the parameters $S_{wc} = 0.2$, $S_{orw} = 0.36$, $S_{org} = 0.1$. The pore size index, $\lambda = 1.66$, and the Land trapping constant C = 1.22. The resulting relative permeability curves are shown in Figure 1. A consistent drainage gas/oil capillary pressure curve was selected with entry pressure P_e = 1.65 kPa, and a special water/oil imbibition capillary pressure curve was generated[8], which would be appropriate to a mildly water-wet system. The capillary pressure curves are illustrated in Figure 2.

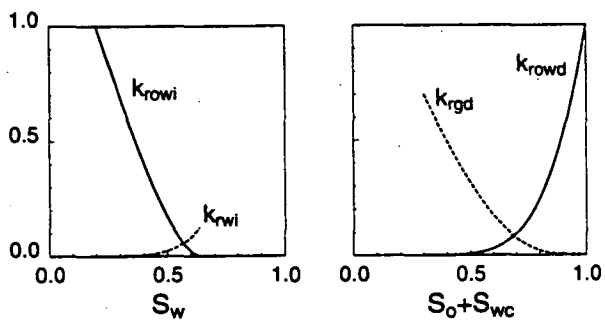

Figure 1: Imbibition water-oil and drainage gas-oil relative permeabilities.

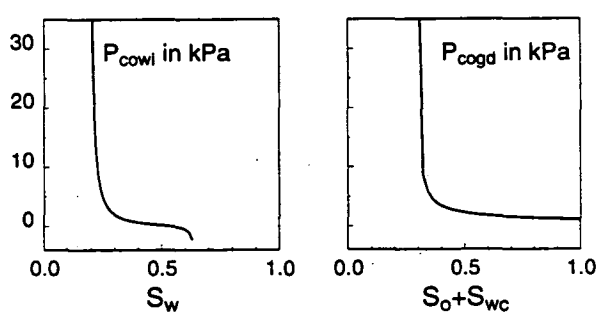

Figure 2: Imbibition water-oil and drainage gas-oil capillary pressures

The simulations have been run with a variety of flow rates, with the base case production rate of $\frac{1}{8}$ x 127 m^3/day ($\frac{1}{8}$ x 800 STB/day, i.e., 5.1% oil pore volume per year). The injection and production rates are matched to give nearly constant average reservoir pressure. Constant oil production rate was maintained until the production well pressure decreased to a chosen lower limit, and thereafter this pressure controls the flow rates. For cases without capillary pressure, the initial oil saturation is uniform with $S_o = 1 - S_{wc}$, but for cases with capillary pressure, initial vertical equilibrium with the drainage capillary pressure curve is used with $S_w = 0.27$ at the bottom of the

reservoir. Over this small range of initial water saturations the drainage and imbibition capillary pressures are nearly equal and there is negligible early water production.

3. Factors in Selecting Stone's Models

Historically preference has been given in reservoir planning studies to using the normalized form[9] of Stone's Method II, since this method does not require selection of a residual oil saturation parameter. Method II expresses the middle phase (oil) relative permeability in terms of the input two-phase water/oil and gas/oil* relative permeabilities as:

$$k_{ro}(S_w,S_g)= k_{rocw}\left[\left(\frac{k_{row}}{k_{rocw}}+k_{rw}\right)\left(\frac{k_{rog}}{k_{rocw}}+k_{rg}\right)-\left(k_{rw}+k_{rg}\right)\right]. \quad (1)$$

Stone's Method I requires judgments on the behavior of a residual oil saturation parameter S_{om}, and is then expressed in normalized form[9] by the equations:

$$k_{ro}(S_w,S_g)=\frac{S_{on}k_{row}k_{rog}}{k_{rocw}(1-S_{wn})(1-S_{gn})}, \quad (2)$$

where

$$S_{on}=\frac{S_o-S_{om}}{1-S_{wc}-S_{om}}, \quad (3)$$

$$S_{wn}=\frac{S_w-S_{wc}}{1-S_{wc}-S_{om}}, \quad (4)$$

$$S_{gn}=\frac{S_g}{1-S_{wc}-S_{om}}. \quad (5)$$

Fayers[1] suggested linear and quadratic functional choices for S_{om}, in the form

$$S_{omq}= S_{orw}-\left(\frac{S_{orw}-S_{org}}{1-S_{wc}-S_{org}}\right)S_g-\varepsilon\left[\left(1-S_{wc}-S_{org}\right)S_g-S_g^2\right] \quad (6)$$

with ε determined using

$$\varepsilon=(a-\frac{S_{orw}-S_{org}}{1-S_{wc}-S_{org}})\Big/(1-S_{wc}-S_{org}), \quad (7)$$

with $a = 0.5$ for a water-wet system. Setting $\varepsilon = 0$ gives the linear form S_{oml}. A comparison between residual oil saturation behaviors for one of his data sets (Figure 1 of Ref. 1) clearly demonstrated that Stone's II can give very pessimistic S_{om} behavior. The ECLIPSE[7] version 3 model primarily used in these studies selects $S_{om} = S_{org}$ in Stone's I, which implies that a low constant value of S_{om} occurs in the presence of any gas saturation. It might seem that this implies very optimistic oil recovery behavior. However, recent work on falling oil film regimes for three-phase flow in water-wet systems (see for example Vizika and Lombard[10] and Blunt *et al*[11]) indicates the possibility of achieving very low residual oil saturations, which would occur if the horizontal displacement rates are not too large. Figure 3 gives a comparison of the residual oil dependencies associated with Stone's II and Stone's I models, where we use the notation S_{omg} for the choice $S_{om} = S_{org}$, S_{oml} for linear dependence, and S_{omq} for quadratic dependence. In our problem Eq. (7) gives $\varepsilon = 0.18$ which implies a small curvature. In order to approximate a more realistic curvature for a falling film regime, we have used $\varepsilon = 1.0$. We will investigate the influence of the choices S_{oml}, S_{omq} for our base case, by using a new feature in ECLIPSE[7] version 4.

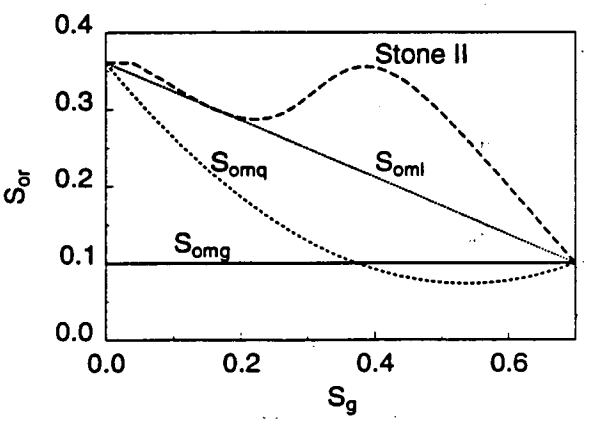

Figure 3: Residual oil saturations (S_{om}) for Stone k_{ro} models

4. Scaling Considerations for Three-Phase Flow

For two-phase flow applications there have been a number of scaling groups suggested which are believed to control the flow regimes in cross sections, which can range from viscous to gravity/capillary dominated, and dictate whether gravity segregated or vertical equilibrium conditions may prevail. Zhou *et al.*[12] have recently completed an analysis of scaling groups, and by making wide ranging comparisons with experiments, etc., have identified regions in which the dominant flow regimes can be related to these dimensionless

* Accurate measurements of k_{rg} and k_{rog} are required at S_{wc}, which are difficult to obtain, and the value of S_{org} is particularly important in Stone's Method I.

groups. The Zhou *et al.* definitions give different dependencies on H/L for the capillary and gravity numbers N_c and N_G, from those recommended by other authors (see for example Shook and Lake[13]). The details of a similar derivation for three-phase flow are given in the Appendix. However, there are very few experimental or computational three-phase results to indicate the flow regimes which might prevail (e.g., when the segregated theory of Virnovsky *et al.* might apply).

There are difficulties in applying scaling theory to a 5-spot pattern, since there are diverging or converging flows near the wells, and very slow flow rates in the more remote reservoir regions. The average width for areal flow in the $\frac{1}{8}$th 5-spot is $L/4$, where L is the well spacing, so we will use this value for determining v_t in the definitions of N_c, N_G in our summary of the simulation results in the next section.

5. Results from Numerical Studies

The primary characteristic evaluated from this work was the variability of the three phase flow region (TPFR), which will depend on the flow conditions and the properties of the two Stone's variants examined (i.e., Stone's II or Stone's I with S_{omg}). For this purpose a grid cell is identified as in TPFR if gas and water saturations allow flow of three phases. From studies in Ref. 4, the selected criteria were $S_w \geq 0.33$, and $S_g \geq 0.051$ and oil flow rate $q_o > 0.002$ m^3/day. Table 1 summarizes the results, where TPFR is expressed as a reservoir volume fraction in percent. The shape factors (see Appendix) have the values $R_h = 16$ for all the cases, $R_v = 20$ for cases 1 to 19, and $R_v = 60$ for cases 20 to 23. All the results show TPFR's which are substantial, in the range 20-75%, with those for Stone's Method II significantly smaller than for Stone's Method I (S_{omg}). When the oil phase becomes trapped at larger oil saturations, the extent of TPFR is correspondingly reduced. The last group of results in the table refer to very slow flow rates (0.25 q_{base}) with large gravity numbers, but there is still no real evidence of complete gravity segregation; the TPFR remains finite. The TPFR's for the base case at one year after gas injection (cases 1 and 2 of Table 1) are compared in Figure 4, for Stone's II and Stone's I – S_{omg}. The position of the TPFR region changes with time, being more in the gas invaded region at early times, and moving down towards the water invaded zone at later times. The introduction of capillary pressure for water causes a modest increase of TPFR at early times, but this is reversed later. The effects on oil and gas production were negligible, and gas capillary pressure has very little effect on saturation distributions.

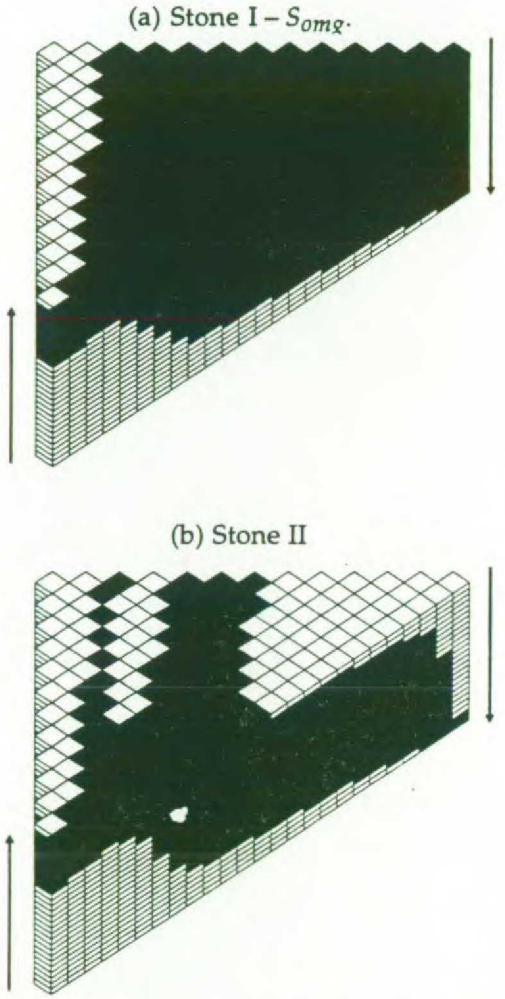

Figure 4: Three-phase flow regions after one year of gas injection, cases 1 and 2 of Table 1.

The oil and gas production rates can be significantly influenced by the choice of Stone's model as shown in Figure 5. For this comparison we used a modified base case with WAG 1:1 injection from $t = 0$. Those calculations were made using ECLIPSE version 4 to obtain additional variants of Stone's I associated with the residuals S_{oml} and S_{omq}. The linear model, S_{oml}, gives oil recovery similar to Stone's II. We believe this occurs because for our particular choice of two-phase relative permeabilities, the Stone's II zero isoperm is quite close to that for the linear model for a range of gas saturations, as seen in Figure 3. The quadratic model, S_{omq}, gives similar behavior to the expected high oil recovery with S_{omg}. The factor of two range in oil production variations is magnified for gas production (an unexpected result), where differences are now seen between the performance

Table 1: Percentage of reservoir in three-phase flow.

	Injection scheme	Stone Model	N_G^w	N_G^g	N_c^w	N_c^g	M_w	M_g	Years after gas or WAG injection		
									1	3	5
1	Gas	I	3.8	7.3	0.0	0.0	0.25	103.7	42.00 %	73.61 %	77.63 %
2	Gas	II	3.8	7.3	0.0	0.0	0.25	103.7	40.52	45.37	24.02
3	Gas	I	2.5	4.8	0.0	0.0	0.25	10.4	33.44	61.82	66.53
4	Gas	I	0.8	1.5	0.0	0.0	1.25	518.5	18.65	12.88	
5	WAG	I	3.8	7.3	0.0	0.0	0.25	103.7	26.10	44.69	39.48
6	WAG	II	3.8	7.3	0.0	0.0	0.25	103.7	17.66	17.70	
7	WAG	I	2.5	4.8	0.0	0.0	0.25	10.4	22.77	39.17	39.25
8	WAG	I	0.8	1.5	0.0	0.0	1.25	518.5	22.72	42.67	47.76
9	Gas	I	3.8	7.3	0.10	0.0	0.25	103.7	48.05	69.70	
10	Gas	II	3.8	7.3	0.10	0.0	0.25	103.7	44.92	40.40	
11	WAG	I	3.8	7.3	0.10	0.0	0.25	103.7	29.78	43.60	37.33
12	WAG	II	3.8	7.3	0.10	0.0	0.25	103.7	18.77	16.69	13.37
13	WAG	I	0.8	1.5	0.10	0.0	1.25	518.5	23.74	44.40	48.88
14	Gas	I	3.8	7.3	0.10	0.11	0.25	103.7	48.09	71.98	76.09
15	Gas	II	3.8	7.3	0.10	0.11	0.25	103.7	44.83	40.33	
16	Gas	I	0.8	1.5	0.02	0.02	1.25	518.5	34.27	67.29	
17	WAG	I	3.8	7.3	0.10	0.11	0.25	103.7	29.82	43.57	37.33
18	WAG	II	3.8	7.3	0.10	0.11	0.25	103.7	18.86	16.75	13.42
19	WAG	I	0.8	1.5	0.02	0.02	1.25	518.5	23.72	44.42	48.85
									Years after gas or WAG injection		
									4	8	12
20	Gas	I	17.6	115.8	0.40	0.0	0.25	25.9	21.40	20.14	
21	Gas	I	17.6	67.2	0.40	0.0	0.25	10.4	32.54	32.83	31.43
22	WAG	I	17.6	115.8	0.40	0.0	0.25	25.9	21.21	8.07	4.45
23	WAG	I	17.6	67.2	0.40	0.0	0.25	10.4	23.62	26.67	13.85

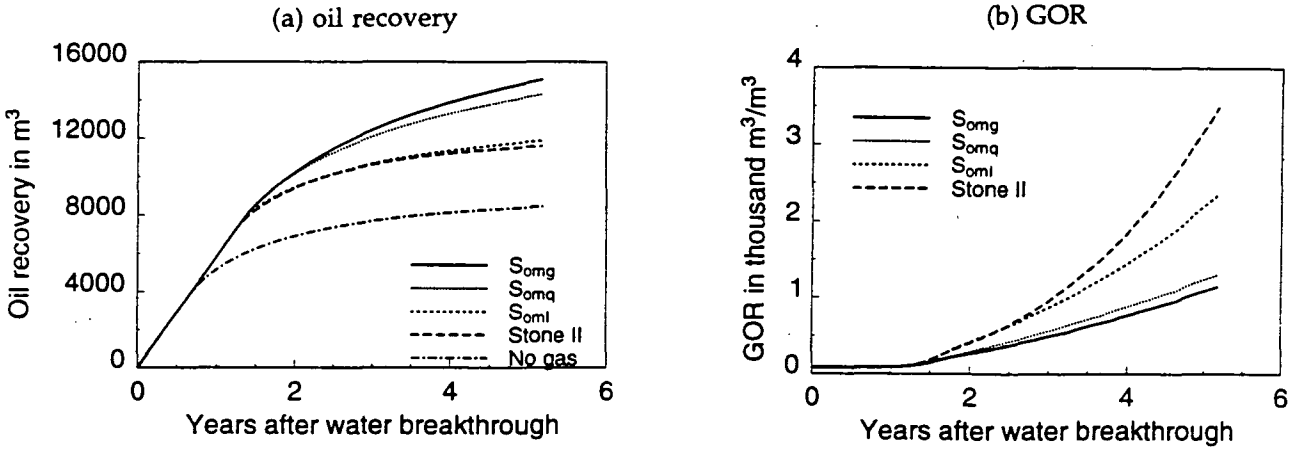

Figure 5: Effect of Stone k_{ro} model for WAG injection from the beginning of simulations.

with Stone's II and S_{oml}. Since high gas production rates are associated with low oil displacement efficiency, there is a significant need to resolve these aspects of three-phase flow behavior.

6. Evaluation of the Use of VE-Pseudos

In the Introduction we summarized potential difficulties foreseen in attempting to simulate

three-phase flow in large, coarsely gridded reservoir models. Perhaps the lack of consistent success in computing pseudo-relative permeabilities for two-phase flow problems has inhibited investigation of the more difficult three-phase situation. An attractive and simple approach which might apply when flow rates are not too large is the use of vertical equilibrium (VE) approximations within coarse grid blocks. Based on the results of the studies for two-phase problems by Zhou *et al.*, we might anticipate that VE conditions could apply when $N_G >> 1.0$. The values of N_C and N_G in Table 1 support the view that gravity should dominate, although capillary pressure may not be important for the gas phase.

The VE condition would require that within any coarse grid block of interval Δz_C, the potential in a phase i must satisfy

$$\frac{\partial \Phi_i}{\partial z} \sim 0. \tag{8}$$

If Φ_o is the reference phase potential, then since $\Delta\Phi_i = 0$,

$$\begin{aligned} \Delta P_{cow} &= (\rho_w - \rho_o) g \Delta z_c, \\ \Delta P_{cog} &= (\rho_o - \rho_g) g \Delta z_c. \end{aligned} \tag{9}$$

If the coarse grid solution in a grid block is giving average saturations $\bar{S}_w, \bar{S}_g$, the VE saturation distribution in that block must satisfy both Eqs. (8) and (9), and

$$\bar{S}_i = \int_o^{\Delta z_c} S_i(P_c) dz / \Delta z_c . \tag{10}$$

Thus, for a particular value of Δz_C, it is a simple matter to compute a tabulation for given values of $\bar{S}_i$, the corresponding upper and lower saturations $\bar{S}_{iu}$ and $\bar{S}_{il}$, and the intermediate values from the P_C-curves which must span the interval Δz_C. For the x-direction of flow, the corresponding VE pseudos then become:

$$\bar{k}_{rix}\left(\bar{S}_i\right) = \int_o^{\Delta z_c} k_{ri}(S_i) dz / \Delta z_c , \tag{11}$$

$i = w,g$, and for the vertical pseudos, depending on the flow direction, the appropriate values are:

$$\bar{k}_{rizu} = k_{ri}\left(\bar{S}_{iu}\right) \text{ or } \bar{k}_{rizl} = k_{ri}\left(\bar{S}_{il}\right). \tag{12}$$

Similar rules can be applied to determine values of $\bar{P}_{cix}$ and $\bar{P}_{cizu}$, $\bar{P}_{cizl}$. Eqs. (10) and (11) ensure that the pseudo-relative permeabilities and capillary pressures for oil and water are monotonic functions of their own saturations. For the oil phase the relative permeability is a function of two saturations (S_w, S_g), thus we need to use $k_{ro}(S_w, S_g)$ in Eq. (11). It is convenient to introduce cut-off values near the ends of the saturation range for S_w and S_g, at which k_{rw}, k_{rg}, or k_{ro} would become so small that segregating flow is no longer appropriate. It is adequate to consider relative permeabilities as being retained as rock curves for saturations outside the cut-off limits. These rules can also be generalized when the reservoir has multiple horizontal geological layers in an interval Δz_C, by using the requirement that P_C must be continuous across a layer interface.

The P_C-curves for water and gas were shown in Figure 2. An immediate difficulty is whether the drainage or imbibition curves should be used for P_{cow}, where in segregating flows it is not clear which is the displacing phase. For purposes of illustration we have taken a single compromise curve for P_{cow} which has a less sharp curvature than the earlier curves, and tends uniformly to $P_{cow} = 0$ at $S_w = 1 - S_{orw}$. The drainage capillary pressure for gas is usually less important and will have $dP_{cog}/\,dS_g \sim 0$ for a significant range of S_g. This shape implies that the VE assumption gives almost segregated flow of gas from the liquid phases and the consequent pseudos for k_{rg} and k_{rog} are almost straight lines. Pseudo-curves for the previous base case problem have been computed using $\Delta z_C = 6.1$ m (20 ft i.e. $\Delta z_C = 5\Delta z$) and have the forms shown in Figure 6. Because the VE assumption implies almost segreated flow of gas, we find for the implied three-phase flow diagram that there is only a very limited range of saturations for which a consistent three-phase flow region can occur. Consequently a pseudo-oil phase relative permeability is not defined in the excluded region. An alternative approach is to construct the oil pseudo relative permeability by applying a Stone's model to the pseudo two-phase curves. The resulting pseudo-k_{ro} isoperms using Stone's I – S_{oml} are compared with the uncorrected Stone's I – S_{oml} results in Figure 7. The differences are very significant, and it seems unlikely that the pseudo-k_{ro} would be useful. In general, any other form chosen for a pseudo-k_{ro} would require a bivariate table lookup procedure for calculating the pseudo-k_{ro}, which is not available in most simulation codes.

In order to analyze the potential applicability of the VE-method we used the baseline data* with the modified P_{cow}, and computed solutions with the original grid, and with the axial grid reduced by a factor of five to give only five vertical intervals. The resulting

* This corresponds to a relatively slow production rate of ~ 5.1% HCPV/year and might therefore conform to the VE assumptions.

oil and gas production histories are compared in

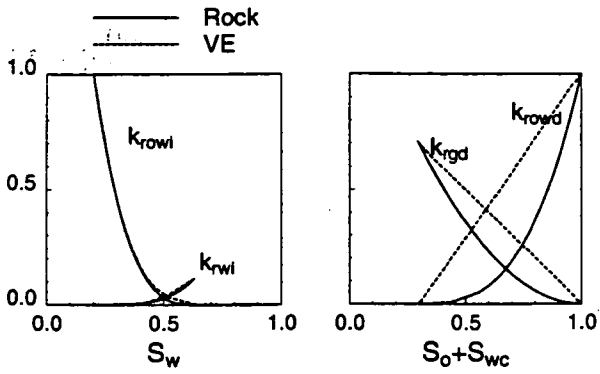

Figure 6: Water-oil and gas-oil rock and VE pseudo relative permeabilities.

(a) rock (Stone I – S_{oml})

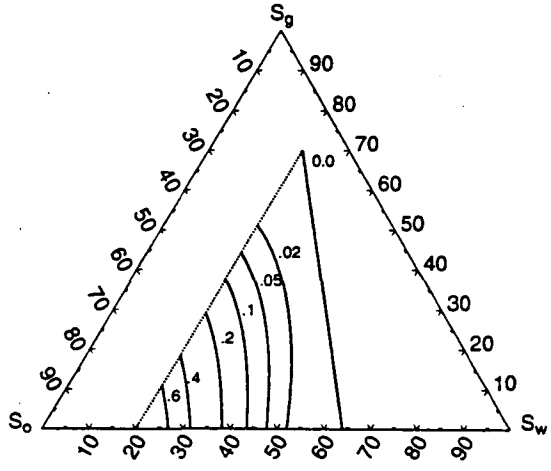

(b) VE

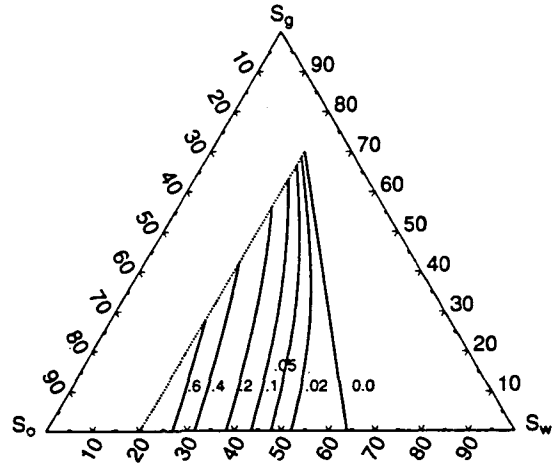

Figure 7: Oil relative permeabilities

Figure 8, which indicates very good agreement using unadjusted relative permeabilities. This implies that the postulated VE-pseudos (Figures 6 and 7b) would perform poorly. Saturation cross plots in the z-direction at various stages of the displacement indicate shapes which are not consistent with the VE-assumptions. An example of the simulated vertical profiles is illustrated in Figure 9, where we also show the corresponding P_c-shapes (consistent with the VE assumption) within coarse grid blocks, matched at the appropriate average saturations. The agreement is poor for the gas phase because it does not show strong gravity segregation.

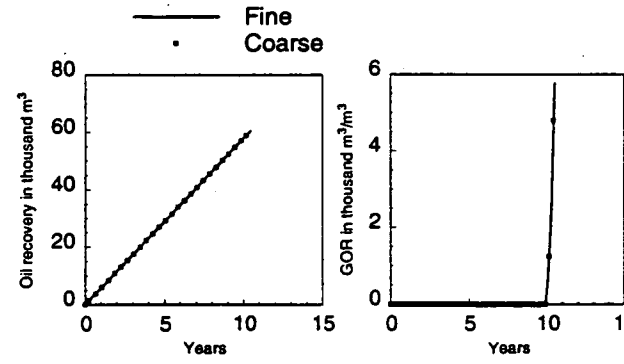

Figure 8: Fine 13 x 25 x 25 and coarse 13 x 25 x 5 grid solutions for case 14 of Table 1.

(a) water

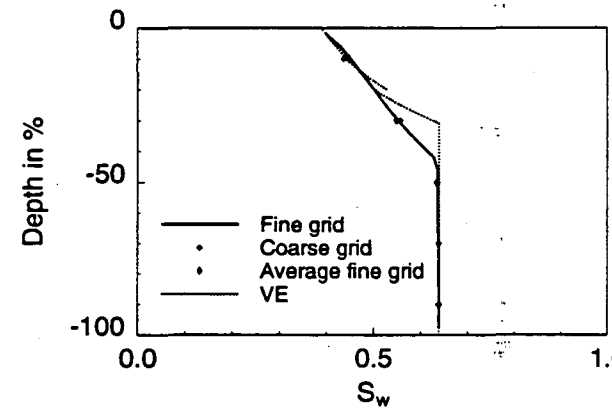

(b) gas

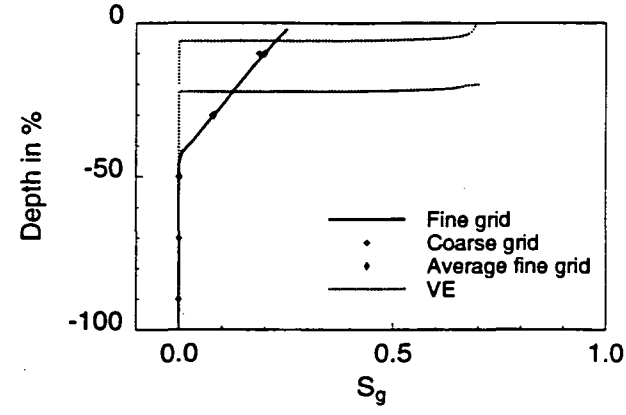

Figure 9: Comparison of vertical saturation profiles for fine and coarse grid solutions and VE, for case 14 of Table 1.

7. Conclusions

We form the following conclusions from these studies:

(i) The three-phase flow region remains large for a range of capillary and gravity numbers.

(ii) Additional oil recovery from WAG displacement can vary by a factor of two, depending on options selected for three-phase relative permeabilities.

(iii) The uncertainty in oil recovery behavior is compounded by a somewhat larger uncertainty in gas production and this acts to worsen the downside assumptions on oil production.

(iv) An acceptable method for calculating pseudos for three-phase relative permeabilities is not available. The VE-method tested here had the attractions of logical simplicity, but its expectations were not confirmed by the nature of the numerical solutions. Fortunately, a coarse grid solution of our test problem appeared to be acceptable without introducing pseudos.

8. Acknowledgements

Thanks are due to D. Giordano and A. Godi, of Agip, who made some of the simulation runs summarized in Table 1. We are also grateful to Prof. Khalid Aziz for encouragement in this work and to the SUPRI-B Simulation Project of Stanford University for funding support (REG).

Nomenclature

C	Land's trapping constant
D	depth
g	gravity constant
H	reservoir thickness
J	dimensionless capillary pressure function
k	permeability
k^*	end point permeability
L	distance between wells
M	end point mobility ratio
N_C	capillary number
N_G	gravity number
P_C	capillary pressure
P_e	drainage entry capillary pressure
q	flow rate
R	shape factor
S	saturation
S_{omg}	constant minimum oil saturation
S_{oml}	linear minimum oil saturation
S_{omq}	quadratic minimum oil saturation
T	time
v	flow velocity ($v = q/(HW)$)
V	Darcy velocity
W	average reservoir width ($L/4$)

GREEK SYMBOLS

Δ	delta
λ	pore size index
μ	viscosity
ρ	density
ϕ	porosity
Φ	potential

SUBCRIPTS

b	base
d	drainage
g	gas
h	horizontal
i	imbibition
n	normalization
o	oil
r	residual
t	total
v	vertical
w	water
wc	water connate
x	Cartesian x coordinate
y	Cartesian y coordinate
z	Cartesian z coordinate

References

[1] Fayers, F.J., Extension of Stone's Method 1 and Conditions for Real Characteristics in Three-Phase Flow, SPE Reservoir Engineering, 1989, **4**, 437-445.

[2] Guzman, R.E., Mathematics of Three-Phase Flow, Stanford University, Ph.D. thesis, in progress.

[3] Virnovsky, G.A., Helset, H.M., Skjaeveland, S.M., Stability of Displacement Fronts in WAG Operations, SPE 28622, proceedings of the SPE Annual Conference, New Orleans, Louisianna, September, 1994.

[4] Kyte, J.R., Berry, D.W., New Pseudo Functions to Control Numerical Dispersion, SPE Journal, 1975, **15**, 269–276.

[5] Coats, K.H., Nielson, R.L., Terhune, M.H., Weber, A.G., Simulation of Three-Dimensional, Two-Phase Flow in Oil and Gas Reservoirs, SPE Journal, 1967, 377-388.

[6] Coats, K.H., Dempsey, J.R., Henerson, J.H., The Use of Vertical Equilibrium in Two-Dimensional Simulation of Three-Dimensional Reservoir Performance, SPE Journal, 1971, **11**, 63–71.

[7] Eclipse 100 Reference Manual, Intera Information Technologies Limited, 1993.

[8] Guzman, R.E., Giordano, D., Fayers, F.J., Godi, A., Aziz, K., Three-Phase Flow in Field Scale Simulations of Gas and WAG Injections, SPE 28897, proceedings of the SPE European Petroleum Conference, London, UK, October 25-27, 1994.

[9] Aziz, K., Settari, A., Petroleum Reservoir Simulation, Elsevier Applied Science, London 1979.

[10] Vizika, O., Lombard, J.M., Wettability and Spreading: two key parameters in oil recovery with three-phase gravity drainage, SPE 28613, proceedings of the SPE Annual Conference, New Orleans, Louisianna, September, 1994.

[11] Blunt, M., Zhou, D., Fenwick, D., Three Phase Flow and Gravity Drainage in Porous Media, accepted for publication in Transport in Porous Media.

[12] Zhou, D., Fayers, F.J., Orr, F.M., Scaling of Multiphase Flow in Simple Heterogeneous Porous Media, SPE 27833, proceedings of the SPE/DOE Improved Oil Recovery Symposium, Tulsa, Oklahoma, April 17-20, 1994.

[13] Shook, M., Li, D., Lake, L.W., Scaling Immiscible Flow Through Permeable Media by Inspectional Analysis, In Situ, 1992, **16**, 4, 311-349.

Appendix

Material balance equations for flow in a three dimensional homogeneous porous media of three immiscible and incompressible phases can be written as:

$$\phi\frac{\partial S_i}{\partial T}+\frac{\partial V_{ix}}{\partial X}+\frac{\partial V_{iy}}{\partial Y}+\frac{\partial V_{iz}}{\partial Z}=0, \quad (13)$$

where $i=o,g,w$, V is velocity, S is saturation, T is time, X,Y,and Z are the Cartesian coordinates.

Let L,W, and H be three characteristic lengths (e.g. length, width, and height), and q be the constant total injection rate, we can define the dimensionless numbers

$$x=\frac{X}{L},\quad y=\frac{Y}{W},\quad z=\frac{Z}{H},\quad t=\frac{qT}{\phi LWH}, \quad (14)$$

$$U_{ix}=\frac{WH}{q}V_{ix}, \quad (15)$$

$$U_{iy}=\frac{L}{W}\left(\frac{WH}{q}\right)V_{iy}, \quad (16)$$

$$U_{iz}=\frac{L}{H}\left(\frac{WH}{q}\right)V_{iz}, \quad (17)$$

where U represents dimensionless velocity. Darcy's law extended to multiphase flow gives the phase velocity

$$V_{ij}=-k_j\frac{k_{ri}}{\mu_i}\frac{\partial\Phi_i}{\partial j},\quad where\quad \Phi_i=p_i-\rho_i gD, \quad (18)$$

where j is either X,Y, or Z, Φ_i is the i phase potential, and D is the depth. Gas and water potentials in terms of oil potentials are:

$$\Phi_g=\Phi_o+P_{cogd}+(\rho_o-\rho_g)gD, \quad (19)$$

$$\Phi_w=\Phi_o-P_{cowi}-(\rho_w-\rho_o)gD, \quad (20)$$

where

$$P_{cogd}=p_g-p_o=P^*_{cg}J_g(S_g), \quad (21)$$

$$P_{cowi}=p_o-p_w=P^*_{cw}J_w(S_w), \quad (22)$$

$$P^*_{cg}=\int_{S_{gc}}^{1-S_{org}-S_{wc}}\frac{P_{cogd}(S_g)dS_g}{(1-S_{org}-S_{wc}-S_{gc})}, \quad (23)$$

$$P^*_{cw}=\int_{S_{wc}}^{1-S_{orw}}\frac{P_{cowi}(S_w)dS_w}{(1-S_{orw}-S_{wc})}. \quad (24)$$

Dimensionless numbers can be constructed by substitution of Equations 18 to 22 into the Equations 15 to 17. As an example consider gas flow in Z direction, substitution of Equations 18, 19, and 21 into Equation 17 gives

$$U_{gz}=-k_{rg}\frac{k^*_{ro}}{k^*_{rg}}M_g\left(R_v\frac{\partial\varphi_o}{\partial z}+N^g_c\frac{\partial J_g(S_g)}{\partial z}+N^g_G\frac{\partial d}{\partial z}\right), \quad (25)$$

where $d=D/H$, and

$$\varphi_o=\frac{WHk_x}{q\mu_o L}\Phi_o. \quad (26)$$

Water and gas capillary numbers that represent a ratio between capillary and viscous forces can be written as follows:

$$N^w_c=\frac{Lk_zP^*_{cw}}{H^2v_t\mu_o}, \quad (27)$$

$$N^g_c=\frac{Lk_zP^*_{cg}}{H^2v_t\mu_o}, \quad (28)$$

The ratio between gravity and viscous forces can be represented by the water and gas gravity numbers

$$N^w_G=\frac{Lk_z\Delta\rho_{wo}g}{Hv_t\mu_o}, \quad (29)$$

$$N^g_G=\frac{Lk_z\Delta\rho_{og}g}{Hv_t\mu_o}, \quad (30)$$

In addition to scaling the forces, it is necessary to scale mobility ratios and shape factors. Water and gas end point mobility ratios are given by:

$$M_w=\frac{k^*_{rw}\mu_o}{k^*_{ro}\mu_w}, \quad (31)$$

$$M_g=\frac{k^*_{rg}\mu_o}{k^*_{ro}\mu_g}, \quad (32)$$

and the vertical and horizontal geometrical shape factors are

$$R_v=\left(\frac{L}{H}\right)^2\frac{k_z}{k_x}, \quad (33)$$

$$R_h=\left(\frac{L}{W}\right)^2\frac{k_y}{k_x}. \quad (34)$$